Adjustment in tumbling rates improves bacterial chemotaxis on obstacle-laden terrains

Sabrina Rashid[1], Zhicheng Long[2], Shashank Singh[1], Maryam Kohram[2], Harsh Vashistha[2], Saket Navlakha[3], Hanna Salman[2], Zoltán Oltvai[2], Ziv Bar-Joseph[1]

[1]Carnegie Mellon University, [2]University of Pittsburgh, [3]The Salk Institute for Biological Studies

The mechanisms of bacterial chemotaxis have been extensively studied for several decades, but how the physical environment influences the collective migration of bacterial cells remains less understood. Previous models of bacterial chemotaxis have suggested that the movement of migrating bacteria across obstacle-laden terrains may be slower as compared to terrains without them. Here, we show experimentally that the size or density of evenly spaced obstacles do not alter the average exit rate of *E. coli* cells from microchambers in response to external attractants, a function that is dependent on intact cell-cell communication. We also show, both by analyzing a revised theoretical model and by experimentally following single cells, that the reduced exit time in the presence of obstacles is a consequence of reduced tumbling frequency that is adjusted by the *E. coli* cells in response to the topology of their environment. These findings imply operational short-term memory of bacteria while moving through complex environments in response to chemotactic stimuli and motivate improved algorithms for self-autonomous robotic swarms.

Bacteria | Chemotaxis | Tumbling

Communication and coordination play a major role in the ability of cells to adapt to ever changing environmental conditions. An example of such coordinated biological process is bacterial chemotaxis. Detailed molecular studies have identified key proteins and signaling pathways involved in this process [1 (and references therein), 2, 3] while other studies have focused on the mode by which individual cells process information and secrete various signals [4] and on pair-wise communication between cells [5]. In previous work, we reported experimental evidence for cell-cell communication that significantly enhances the chemotactic migration of bacterial popula-tions. Specifically, we have found that *E. coli* cells respond to a gradient of chemoattract-ant not only by biasing their own random-walk swimming pattern but also by actively secreting a strong chemoattractant into the ex-tracellular medium that amplifies the migration of cells distant to the attractant source. Although no specific ligand has been fully identified, a number have been hypothesized to be involved in the secretion process [6].

To gain insight into the ecosystem-level organization of chemotaxis, mathematical models have been developed to de-scribe the collective behavior of cells [7-11] and simulations in-dicated that these capture several aspects of the observed be-havior [12-13]. One of the first models developed for bacterial chemotaxis is the Keller-Segel PDE model [11] that describes the concentra-tion profiles of bacteria and attractant over time using coupled differential equations. Later models were based on experiments from Brown and Berg et al. [14]. These models made the dura-tion of bacterial trajectory (following a tumbling step) at a specific direction a function of the perceived attractant gradient [9-10]. However, these studies did not account for the cooperative aspects of foraging bacteria. More recent models, developed by Shklarsh et al [12] and Singh et al [13] attempted to mathematically and computationally account for the collective aspects of this process either by using an extended differential equations mode or by modeling the process as a distributed gradi-ent descent (DGD). Simulations based on these models showed that communication can indeed improve the average speed in which cells reach the attractant source.

In addition to these mathematical models developed to explain chemotaxis, this process also serves as the basis for several distributed computing swarm based methods. For example, robotic swarm methods for searching for trapped victims in emergency situations are often based on chemotaxis [15-16]. In such applications, robots integrate signals from victims (either based on smell or sound) with visual information from neighboring robots to determine their search route.

While these mathematical and computational models are based on studies that have considered cell migration in response to chemoattractants, relatively little work has focused on the ability of cells to operate in more complex environments, including when faced with obstacles and noise. Previously developed models for collective bacterial behavior do not take into account the impact, and feedback, from the physical environment on the cell state. For example, when bacteria traverse obstacle-laden surfaces, current models indicate that exit times would increase with increased obstacle coverage since obstacles limit the ability of cells to select an optimal route.

To test if this is indeed the case, we performed experiments in which we studied the move-ment of *E. coli* cells in microfluidic chambers containing physical obstacles. We varied the obstacle size or the overall surface coverage by obstacles. Contrary to predictions of current models, we found that average bacterial exit times remain nearly constant regardless of the specific obstacle coverage or size. We found that two changes in one of

---

Significance

Bacterial chemotaxis is the process of bacterial migration in the direction of food and/or chemo-attractant, and away from chemo-repellents. Several models have been proposed for this process and these predict that their migration across obstacle-laden terrains would be slower when compared to terrains that do not contain obstacles. However, our experiments show that the presence of obstacles does not alter the average time it takes E.coli cells to reach the food source. We show, both theoretically and experimentally, that a modified model that relies on adaptive movement following collisions with obstacles accurately explains this surprising result. These findings imply operational short-term memory of bacteria and motivate improved algorithms for self-autonomous robotic swarms.

Reserved for Publication Footnotes

137
138
139
140
141
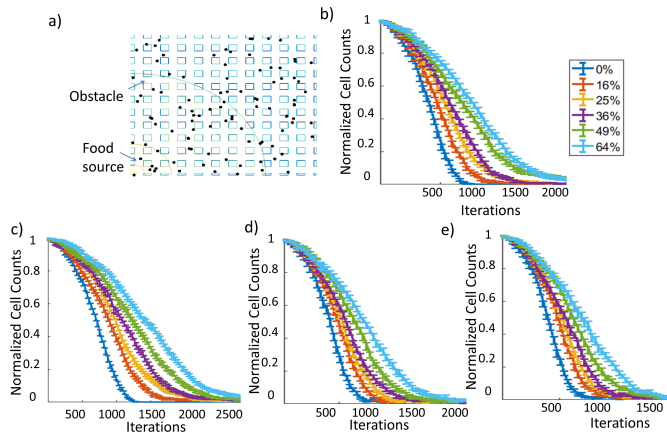142
143
144
145
146
147
148
149
150
151
152

Fig. 1. Simulation results of current chemotaxis models. We tested several different bacterial chemotaxis models simulating cells faced with varying obstacle coverage within an attractant gradient. All models predicted much slower escape times when the environment contains more obstacles. **(a)** Terrain model for simulations of bacterial food search. Obstacles are placed in a grid and the attractant source is at the bottom right corner, as in the experimental setup. Black dots denote bacteria (agents) **(b)** Adaptive step size model based on Brown-Berg experiment [14, 17] **(c)** Keller-Segel model [11] **(d)** Shklarsh model [12] **(e)** DGD model [13]. It is evident, that all models predict the fastest exit rate of cells in the absence of any obstacles.
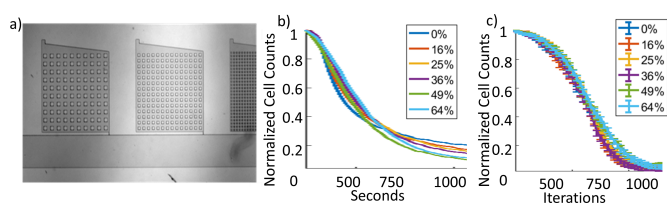

Fig. 2. Experimental results and revised DGD model. We performed experiments to test the accuracy of the predictions made by all models. **(a)** Design patterns of a microfluidic device with different obstacle size. Other designs tested include those with the same obstacle size but different coverage (See SI Appendix, Fig. S1). **(b)** Total cell count of YFP-labeled, wild-type *E. coli* RP437 cells in the microchambers as a function of time, after applying a M9CG chemotaxis stimulus. Note the difference between the experimental results and simulation results from Fig. 1. **(c)** Simulations using the revised DGD model for the same settings. Changing the secretion model and adjusting tumbling rates based on the environment the updated DGD model leads to results that are concordant with the experimental results.

the theoretical models can explain the observed behavior. The first is a change in the communication protocol that limits the sending of messages (secreted signaling molecules). The second modification was an adaptive change in the tumbling rate based on the presence and coverage of obstacles. We tested the latter prediction and found that higher obstacle density indeed leads to adaptively lower tumbling rates over time.

Results

Analysis of existing chemotaxis models

We tested several existing models of bacterial chemotaxis by examining their predicted exit time (time to reach the attractant source) in several topologies with regularly spaced obstacles (Fig. 1a). These include the Keller-Segel model [11] and models based on Brown & Berg [14,17], which focus on individual cell movement in response to chemoattractant. Another model we tested was a differential equations (DE) model by Shklarsh et al [12] that divides the area around each cell into three different compartments and allows for both physical and chemical communication between cells, where depending on their distance, neighboring cells either attract or repel each other (Methods). Finally, we
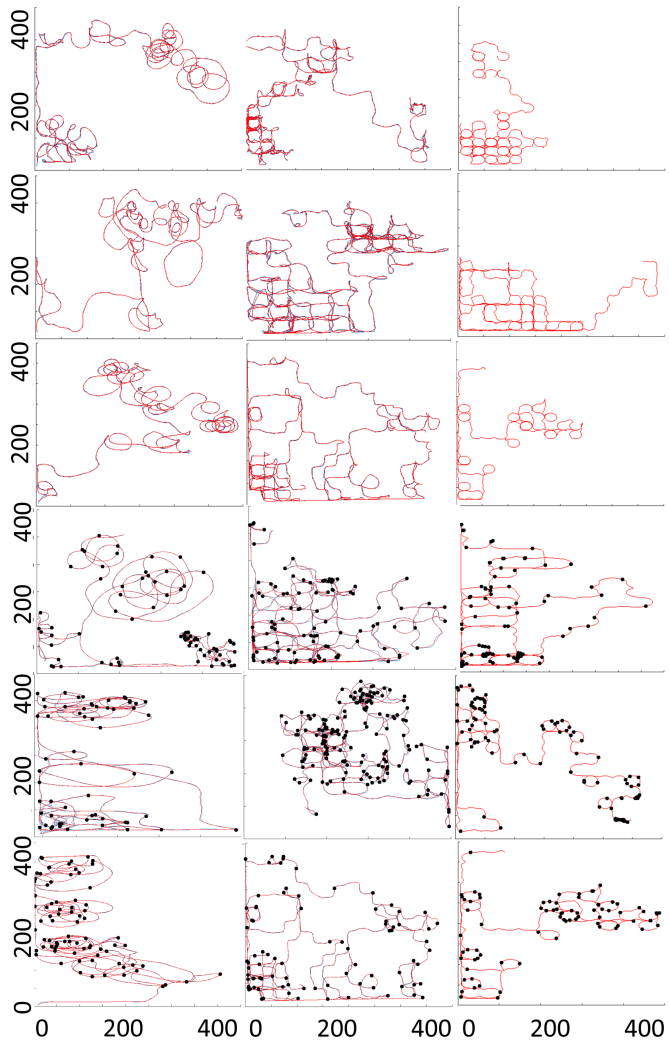

Fig. 3. Single cell trajectories under different obstacle coverages. Left column (top 3 rows): Trajectories of cells when no obstacles are present. Middle column (top 3 rows): Trajectories with 64% of the area covered by square obstacles. Right column (top 3 rows): Trajectories with 64% of the area covered by round obstacles. Note, the grid like trajectories of individual cells are due to the obstacles. Bottom 3 rows: Additional trajectories without (Left column) and with (Middle column (square), Right column (round)) obstacles, this time with the identified tumbles marked by black dots. As discussed in the text and in Fig. 4, the analysis identifies more tumbles in the 'no obstacle' cells even though they are much less constrained than the 64% group. The food source is located at the bottom left corner at (0,0).

considered a Distributed Gradient Descent (DGD) model that allows for a continuous set of messages to be exchanged among cells and for cells to combine their internal sensing (based on the gradient they observe) with the messages received from other cells to determine their next move [13]. Figure 1b-e depicts simulation results for these models on environments containing different numbers of regularly spaced obstacles of the same size (see Supporting Movies). In these simulations, the area covered by the obstacles ranges from 0% to 64%. As can be seen, all models predicted that with 0% coverage (no obstacles) bacteria would reach the attractant source faster than in the presence of increasingly higher obstacle coverage.

Experimental results contradict model predictions

Given the simulation results, we next asked if these models can indeed qualitatively describe the collective migration of *E. coli* cells in complex environments. In addition to model validation, such experiments may provide new insights and can help
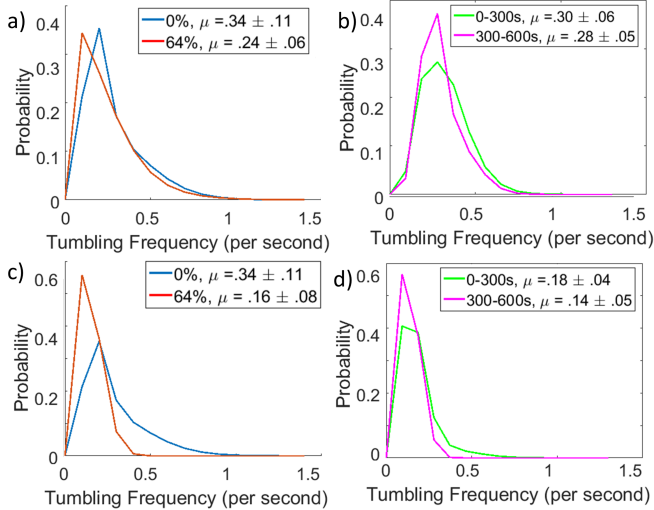
Fig. 4. Distribution of tumbling frequency under different obstacle coverages. (a,c) Distribution and average of tumbling frequency (tumbles per second) for two different obstacle types: **a)** 0% (red) and 64% square obstacles (blue), **c)** 0% (red) and 64% round (blue). A shift in the mode to the left (lower) for the 64% case is evident, indicating that cells may indeed be learning to reduce their rates. **(b,d)** Distribution and average of tumbling frequency (tumbles per second) for cells in 64% **(b)** square, and **(d)** round, obstacle covered environments at two different times: early (first half of trajectory, green) and late times (second half, pink). Cells reduce their average tumbling frequency over time, especially if these rates are high to begin with (right hand side).
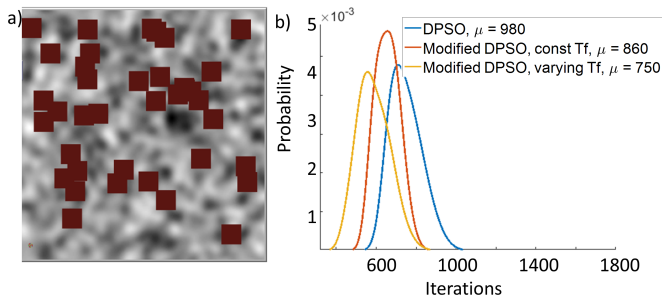

Fig. 5. Application of adaptive tumbling frequency method for swarm robot search task. a) Terrain used in one of the NetLogo simulations. Grey shades correspond to attractant distribution. Red squares are randomly placed obstacles. See SI Appendix (Fig. S14) for parameters used in the simulations. b) Distribution of search time in DPSO and Modified DPSO with constant and varying tumbling frequency over 50 independent trials. denotes the average search time in each setting.By adjusting tumbling frequency based on the terrain the modified DSPO method improves search time.

further improve algorithms and analysis [18-19]. To this end, we designed and fabricated a microfluidic device to test the chemotaxis of *E. coli* cells in terrains without and with obstacles of different sizes and coverage (Fig. 2, SI Appendix (Methods, Fig. S1)).

We first performed experiments in which we followed cells in environments with 0%, 16%, 25%, 36%, 49% and 64% of total area covered by obstacles of identical size (50 µm²) (Fig. 2a). We used either a complex medium (M9CG) (Fig. 2b), where the attractant gradient was created by the bacteria depleting the nutrients in the rectangle chamber while fresh nutrients are supplied through one of the rectangle's corners, or a single attractant medium (200 µM aspartate [Asp] in M9-G), where 200 µM aspartate was supplied continuously through one of the chamber's corner. (SI Appendix, Fig. S2, S7). To determine the impact of the various obstacle types on the time it takes *E. coli*

cells to reach the attractant source, we measured the change in the fraction of cells remaining in the chamber as a function of time. In contrast to predictions by all models (Fig. 1b-e), *E. coli* cells displayed no substantial difference in their average exit times between different overall coverages. In fact, regardless of the overall surface coverage *E. coli* cells exited the microchambers at nearly identical rates (Supporting Movie 1). We also tested the migration of cells using microchambers containing different obstacles' shape (round instead of square) with the same surface coverage as before and observed the same results, as well as different obstacle sizes but constant total surface coverage (25%). We determined that variation in obstacle size and shape does not affect the bacteria's chemotactic migration towards the attractant source (SI Appendix (Figs. S4,6), Supporting Movie 2).

Revising the DGD model to fit experimental results

Given the disagreement between experimental and simulation results we further considered the DGD model to determine if any specific changes to it can result in better agreement with the experimental data. We tested several different possible changes (Methods) based on either previously implied molecular behavior (for example, when do cells secrete the chemical attractant?) or changes that affect parameters that are used by the model (for example, tumbling frequency, message weight when integrating information, etc.). For each of the changes we re-run the simulations and compared their output to the experimental results. We identified two key changes that help improve the match to experimental results. The first affected the messages sent by each cell (secreted signaling molecules). While prior models assume that cells secrete such signaling molecules continuously, we found that limiting the release of the attractant to only when a cell observes an improvement in the chemo-attractant gradient leads to better performance in the more complex environments. This change in the model is supported in part by our recent study where we observed that bacteria indeed secretes an attractant in response to sensing an external attractant gradient [6].

The second and more surprising model change was related to a reduction in tumbling frequency based on the environment the cells occupy. We observed that reducing the tumbling frequency based on the number of times a cell is unable to proceed in a given direction due to obstacles in its path, leads to much faster exit times in the higher coverage environments (see Methods for mathematical and computational details, which are based on feedback loops). With these changes, the simulation results of the updated DGD model exhibited qualitatively good agreement with the experimental results (Fig. 2c and SI Appendix (Fig. S4), Supporting movies 3 and 4). We also tested the impact of these changes on another prior model (Shklarsh model). However, simulations based on the updated Shklarsh model till did not agree with experimental results (SI Appendix, Fig. S8). Beyond the differences in assumptions between the DGD and the Shklarsh models (SI Appendix), the Shklarsh model assumes that cells can only use the orientation of nearby agents to update their own direction (introducing a cutoff to determine 'nearby'). In contrast the DGD model uses a continuous version of distance rather than orientation which as we show leads to better agreement with the experimental results.

Experimentally testing model predictions

The revised model leads to two predictions about the behavior of *E. coli* cells in complex environments. First, it predicts that tumbling is reduced when the obstacle coverage increases. Second, it predicts that such reduction is based on feedback, and thus over time, we expect a reduction in tumbling in cases where cells encounter an environment in which a large fraction of the surface is covered by obstacles. The first prediction is intuitive. When a cell encounters a barrier, it moves parallel to it, which leads to a reduction in tumbling frequency [20]. However, the second prediction is surprising and we are not aware of prior work

describing it. Such change implies that bacteria may have a long term adaptation mechanism.

To test these predictions we analyzed the movement of individual cells in different environments by tracking their trajectories (Methods). The tracking algorithm links a cell in a frame with the closest cell in the next frame within a maximum dis-tance, which was set to 10 pixels ($\sim$23 μm). Tracking was performed for three different terrains: An environment with no obstacles (0% cover-age), with 64% square obstacle cover-age, and with 64% round obstacle cover-age. Fig. 3 displays a number of representative cell trajectories for these environments. Given the trajectories of each cell, we next analyzed their tumbling frequencies T_f. We define a `tumble' when the angular movement of a cell is above a certain threshold (Methods). Since cells complete a tumble over a period of time, we based the tumble calls on multiple consecutive frames. From the point of origin in the movie, or the end of the previous tumble, we have computed cumulative angular movement in the subsequent frames. When the cumulative angular movement reaches the pre-defined threshold, we call it a tumble and up-date the point of origin at the detected tumble location. This is repeated until the tracking for the cell is completed (Methods). Detected tumbles for these environments are shown in Fig. 3 (bottom three rows). As can be seen, while the 64% coverage environments are more constrained, cells seem to perform fewer tumbles. In contrast, even though they are not facing any specific limit on their movement, in the unconstrained 0% environment cells seem to tumble more. Fig. 4a,c quantifies these differences and presents the tumbling frequency distributions for the 0% and 64% environments. Tumbling frequency is computed by dividing the number of tumbles in each track by the duration of tracks in seconds. Distribution is calculated using tumbling frequencies for all the cell tracks. As can be seen, the average tumbling frequency is lower in the 64% coverage setup by $\sim$30% when compared to the 0% coverage, as predicted by the revised model. Similarly, Fig. 4b,d compares the tumbling frequency for the earlier frames in the 64% environment to those in the later frames/times. These distributions are only based on cells that were present in both the earlier and later subsets of frames. Again, as predicted by the model we see a decrease ($\sim$10%) in the tumbling frequency over time indicating that cells can indeed adjust their tumbling rates based on their environment. We observe similar tumbling distribution plots from simulation of the revised DGD model (SI Appendix, Figs. S10, S11).

We have also performed global analysis using mean square displacement (MSD) to model tumbling in the single cell tracks. MSD as a function of time exhibits 2 distinct regimes. In the short time scale it exhibits a power-law behavior ($\langle x^2 \rangle \propto t^\alpha$), with power α=2, which reflects the ballistic nature of the motion at that scale. In the long time scale the MSD exhibits a diffusive behavior, where $\langle x^2 \rangle$ is proportional to t. The transition time between these two regimes t_e is thus the average lifetime of the ballistic motion, i.e. it is the average time of a straight run or the inverse of the tumbling frequency (see also Methods) [21]. The MSD analysis results (SI Appendix Fig. S12) and are in good agreement with our previous findings. We find that t_e is larger in terrains with obstacles (i.e. lower tumbling), and that in the presence of obstacles it increases with time indicating that the tumbling frequency decreases in time. Note that this change in t_e or the tumbling frequency in time cannot be attributed to the bacteria getting closer to the chemo-attractant source and therefore sensing a stronger gradient, since such effect will be observed in the microchambers without obstacles as well. The inferred tumbling rate, every 3-5 seconds, is higher than what is typically observed in homogenous environments. This relatively longer run is likely the result of the use of a specific attractant, aspartate, which was shown to lead to less frequent tumbling [36].

Discussion

Several studies have focused on organism and cell movement. For example, in [22] the authors model ants' movement and in [23] the authors model zooplanktons' movement response to light source. Other studies have attempted to model movement of bacteria in response to a chemical stimulus [24-26]. However, as we showed, these models cannot accurately predict bacterial behavior in complex environments. Bacterial cells face many obstacles in their natural environments. Whether trying to reach a nutrient source, or host cell for pathogens, bacteria often have to navigate through confounded terrains. *E. coli*, for example, naturally inhabits the gastrointestinal tract, which is a complex environment and can impose complicated topology with physical obstacles. Therefore, it is likely that their behavior in such environments has evolved to minimize the time to reach an attractant nutrient source (e.g., aspar-tate). To uncover likely mechanisms used by bacteria to reduce search time in such complex environments we consid-ered several possible changes to mathematical models of such behavior that can lead to observed exit times of cells. We found that in addition to limiting the secretion of cell-cell signaling to times when the cell is moving up a gradient, a key change that greatly improves exit times is reducing tumbling rates based on the number of times the cells encounter a physical obstacle. In other words, cells seem to "learn" (form short term memory of) the complexity of the environments they are in and adjust their tumbling rates accordingly. While the control of such "learning" mechanism is not known, adaptation to the environment is very common in bacteria. For example, bacteria adapt their sensing ability to their surroundings as they move up an attractant (or down a repellent) gradient, such that they are always able to sense a relative improvement in the conditions [27]. Reduction in tumbling frequency may be controlled through the cell's mechano-sensing apparatus, whose effects has been reported, but its control mechanism is yet to be discovered [28-29].

Applying the changes mentioned above, leads to models that mimic observed behavior under a wide range of obstacle coverages. While we still observe some differences between ex-periments and simulations, these are likely the result of cells that get stuck to the plate, or due to changes in the external gradient over time. While most cells manage to escape before there is a significant change in the gradient, at some point the microchamber becomes saturated with the external signal pre-venting remaining cells from escaping (for more details of the gradient change over time see [6]). However, this difference does not impact the conclusions of our modeling and experimental results which indicate that the decrease in tumbling rate is the likely reason for the faster than expected) exit of most cells.

To test if the model predictions indeed reflect bacterial be-havior we have tracked single cells in settings with and without obstacles. These experiments revealed that when faced with ter-rains that are covered by a large number of obstacles (64% total surface coverage) cells indeed reduce their overall tumbling rates when compared to those observed without any obstacles (0% coverage). Further, we have shown that this behavior is indeed adap-tive. Even for the 64% coverage case we observe a reduction of tumbling rates over time with higher initial tumbling, which is reduced as the cells encounter more and more obstacles. We note, however, that in our analysis, we do not distinguish between tumbling due to intracellular mechanisms or due to the physical environment. This is because both would have the same effect on the overall motion of the bacteria. However, the fact that there is a change in the tumbling frequency over time in the same terrain indicates that the intracellular control mechanism is influenced by the physical environment, which does not change over time. As for the setup, we are only considering bacteria movement in liquid media where passages between obstacles are at least one order of magnitude larger than the bacteria themselves. In

much smaller passages, such as in semisolid agar, the bacteria behavior may be different. Future studies are also required to identify the molecular mechanism by which *E.coli* cells control such adjustments in their tumbling rates.

An interesting question that this study raises is how the migration of bacteria away from repellents would be influenced by physical obstacles. The consensus in the field is that the bacterial migration away from repellents is driven by the same mechanism as its migration towards attractants. However, an important distinction should be made here. Our results, as well as previous studies [6] point to a cell-cell communication mechanism in which secretion of the attractant is triggered by the sensing of the external signal. This might be similar when bacteria are moving down a repellent gradient if the secretion is triggered by any improvement in the environment. However, if it is triggered by the sensing of a specific chemical, then one would expect that the migration of bacteria down a repellent gradient will differ significantly from the pattern observed here. This question remains open for future studies.

Reasoning under uncertainty, in which a collection of agents needs to reach a common goal while each has access to limited information is also of major interest in the Artificial Intelligence (AI) community. Current algorithms for this problem utilize robotics swarms that often operate in noisy and complex environments [15]. However, most AI algorithms for this task do not allow feedback from the environment or topology to adjust the hyper-parameters used in the algorithm. To test whether the idea of reduced tumbling in complex environments can improve swarm based searches we used a simulation environment implemented by NetLogo [33] (Methods). A recent benchmark paper [35] identified the Darwinian Particle Swarm Optimization (DPSO) [34] as the most efficient current method in avoiding local minima in these distributed search tasks. We compared three possible search methods: No tumbling, fixed tumbling, and adaptive tumbling similar to the behavior observed for bacterial cells. As can be seen, we observe an improvement (reduction in search times) when using adaptive tumbling in noisy environments (Figure 5). These results show, that adopting insights based on bacterial coordina-tion can suggest new directions to improve the performance of these algorithms. More generally, our results provide additional support to the usefulness of studies that attempt to determine what and how biological processes compute, and in turn use the results to improve computa-tional methods [18-19].

Methods

Bacterial strains and growth conditions

The wild-type *E. coli* K12 strain RP437 that constitutively express yellow fluorescent protein (YFP) from the plasmid PZA3R-YFP or mCherry from the plasmid PZA3R-mCherry, both of which containing chloramphenicol resistance, were used. Strains were first grown overnight at 30°C with strong agitation (240 rpm) in M9 minimal medium supplemented with 1g/L casamino acids and 4g/L glucose (M9CG) and appropriate antibiotics. Cultures were then diluted 100 fold in fresh M9CG and grown at 30°C until early exponential phase, optical density at 600nm (OD600) of 0.1-0.2. Prior to loading the bacteria the cultures were centri-fuged, washed, and resuspended in fresh testing medium. Testing media used were either M9CG or M9G (M9 minimal medium supplemented with 4g/L glucose and 500 g/mL each of L-threonine, L-leucine, L-histidine, L-methionine, and thiamine).

Microfluidic device

The design and fabrication of the microfluidic devices used were as described before [6]. Briefly, the microfluidic device (Fig. 2a and SI Appendix, Fig. S1) contains eleven consecutive microchambers that are connected to a wide channel through a 5μm-wide and 40 μm-long inlet channel that allow the introduction of *E. coli* cells and media into the microchambers. Excluding their nook area, the microchambers are 10 μm high, 1 mm wide and 1 mm long and contained evenly distrib-uted square obstacles. The microdevice was fabricated by standard soft lithography. See SI Appendix for details.

Time-lapse imaging

Migration of YFP-expressing *E. coli* cells were recorded in fluorescence mode using a fully automated inverted microscope (Zeiss AxioObserver Z1), equipped with a motorized x-y stage (Applied Scientific Instruments). Time-lapse movies were acquired at a rate of 2 frames/min in population level experiments and 3/10 (square / round obstacles) frames/second in single cell

tracking experi-ments using a CCD camera (Zeiss AxioCam MRm) at room temperature (26°C). Movies were analyzed using the ImageJ software. The cells inside the microchambers in each image were counted automatically using Cellprofiler [30]. Analysis of the movement of individual cells was performed with Track-mate, a Fiji plugin for single particle-tracking [31]. See SI Appendix for complete details.

DGD model for bacterial chemotaxis

We tested several prior models of bacterial chemotaxis including those that focus on individual cells and those that consider communication be-tween cells. These include the Keller-Segel model [11], the individual chemo-tactic movement model based on Brown-Berg experiment [14, 17], the Shklarsh model [12] and the DGD Model [13]. Details about these models are in SI Appendix. We only discuss here the DGD model since it is the model we extended to account for adjusted tumbling rates.

In the DGD model the movement of an agent i at time n is a function $d_i(n)$ of two quantities: its own sense of direction $\theta_i(n)$ (based on the chemical gradient), and the locations and movement directions of other migrating cells. In this dynamic interaction network of migrating bacteria, nodes correspond to bacteria, at some current location $x_i(n)$, and edges, represent-ing physical distance, exist between every pair of cells. The DGD model updates $d_i(n)$ based on individual belief and the beliefs of neighbors, while using simple messages (formalized below).

The model assumes that individual cells follow a chemical gradient of food source by decreasing their (random) tumbling angle at high concen-trations and thus largely move in the direction of the attractant. Specifi-cally, bacteria perpetually move in a direction that they repeatedly perturb randomly. The magnitudes of these perturbations are inversely related to the change in the attractant concentration between iterations, with the approximate effect that the agent/cell continues to move in gradient direction. Formally, under these assumptions, at time, n, cell i changes its direction by an angle $\theta_i(n)$, which is a function of $c_i(n)$, the difference in food concentration between the current and previous time steps. Specifically, the new tumbling angle $\theta_i(n)$ is sampled randomly from a Gaussian distri-bution $\theta_i(n) \sim N(\theta_i(n-\Delta n); \sigma(\Delta c_i(n))^2)$ centered at the previous angle $\theta_i(n-\Delta n)$, with the variance $\sigma(\Delta c(n))^2$ given as:

$$\sigma\big(\Delta c_i(n)\big)^2 = \begin{cases} 0, & \Delta c_i(n) \geq 0 \\ \pi, & \Delta c_i(n) < 0 \end{cases}$$

Thus, based only on its own perception of the food gradient, the ith agent updates its location $x_i(n)$ according to

$$x_i(n + \Delta n) = x_i(n) + s_i(n)\, \Delta n;$$

where $s_i(n)$ is the unit vector in the direction of the movement.

$$s_i(n) = (cos(\theta_i(n)); \sin(\theta_i(n)))$$

The above equation is based on individual sensing only. We denote by $v_i(n)$ the aggregate of all secreted chemicals by neighboring cells (see SI Appendix for details). At each step $v_i(n)$ is updated, as follows:

$$v_i(n) = D_{L,T}\Big(\sum_j \frac{\exp(Ca(x_i(n)-x_j(n)))|x_i(n)-x_j(n)|}{x_i(n)-x_j(n)}\Big)$$

$D_{L,T}$ is a discrete thresholding operator parameterized by L, a positive integer denoting the number of possible messages, and T, an upper bound above which all messages are treated as the highest value possible (see [32] for the exact construction of this "stone-age computing" threshold, which has been used in ant migration models). Ca is a positive diffusion constant, determining how quickly the location signal diffuse from the source agent. Under this model, bacteria communicate the attraction information using only log2 L bits. The model also includes a physical repulsion term. If an agent physically interacts with another agent it moves in the opposite direction to where it came from regardless of the other information it has. Hence the direction will be updated, as follows:

$$v_i(n) = -\sum_{j \in RR} x_j(n) - x_i(n)$$

Where RR is an influence radius that is related to the physical size of the agents and their speed such that agents cannot reach agents outside of RR in a single round [12]. Finally, the agent combines the messages it received with its own observation $s_i(n)$, resulting in the following modification of equation (2):

$$x_i(n + \Delta n) = x_i(n) + \left(\frac{v_i(n)}{|v_i(n)|} + w s_i(n)\right).\Delta n$$

w is a scalar constant. A schematic layout of the original DGD model is presented in the SI Appendix, Fig. S9a.

Revising the DGD model to fit experimental observations

Chemotaxis models [12,13] assume that the cells communicate via chemical secretion at all points of their search, irrespective of their individual sensing of the attract-ant gradient. However, recent observations suggest that this may not be the case. Instead, cells only signal (via secretion of amplifying signaling molecule(s)) when they are moving in the right direction (i.e., positive gradient change) [6]. We have thus revised the model so that only messages from cells with positive gradient change are allowed. Denote by $\Delta c_i(n)$ the gradient change perceived by cell i.

We update eq 4, as follows:

$$v_i(n) = D_{L,T}\left(\sum_{j,\Delta c_j > 0} \frac{\exp(-(\mathcal{L}_\partial|x_i(n)-x_j(n)|)(x_i(n)-x_j(n)))}{|x_i(n)-x_j(n)|}\right)$$

The revised model also allows cells to adjust their tumbling frequency according to their perception of the environment. We assume that cell i iteratively updates (via a feedback loop) its tumbling time, denoted t_i as follows (note that t_i is tumbling time in seconds, tumbling rate is $1/t_i$):

$$t_i(n) = (1+f)^{nb_i(n)} t_i(n-1)$$

Here, $nb_i(n)$ is the number of times agent i has encountered an obstacle before iteration n. f is a constant.

This adaptive formulation of t_i change throughout allows the cells to adjust their movement in high obstacle coverage. When a cell encounters an obstacle, we assume that it remains in its current location (velocity 0) and then adjusts its direction to align with it until its next tumble.

Using the new rate we update eq 1 as following: change below according to text above

$$\sigma\big(\Delta c_i(n)\big)^2 = \begin{cases} 0, & \Delta c_i(n) \geq 0 \\ \pi, & \Delta c_i(n) < 0 \;||\, \delta_i(n) \geq t_i(n) \end{cases}$$

Finally, we model variable cell sensing abilities (corresponding to difference within cell popula-tions) by adding an additional Gaussian noise term to $\Delta c_i(n)$:

$$\Delta c_i(n) = N(\Delta c_i(n); \Delta c_i(n)(1-\alpha_i))$$

Here α_i denotes $i's$ specific sensing ability, which we assume varies between 0 and 1 (0 denotes the lowest sensing ability, i.e., cells cannot perceive the food gradient at all). A schematic layout of the revised DGD model and sensitivity analysis of its parameters is shown in SI Appendix (Fig. S9, Table S2).

Computing tumbling rates

To compute tumbling frequencies (TFs) we first define a 'Tumble' when the angular movement of a cell reaches a certain threshold (80° in this paper, results are robust to the selection of the threshold). Since cells complete a tumble over a period of time, we analyze multiple consecutive frames (frame rate: 10/3 frames per second) to detect a complete tumble (Formal algorithm is given in SI Appendix, Table S1). We take an iterative approach to count the total number of tumbles in a single cell track. From a point of origin in the track we compute cumulative angular movement in the subsequent points. When the cumulative angular movement is above a certain threshold, we define it as a tumble and update the point of origin at the detected tumble location. We again compute cumulative angular movements until the cell exits or the movie ends. Due to noisy measurement we sometimes observe multiple large angular movements in a very short time span that do not represent actual tumbles and falsely increase the total tumble counts. To avoid that, for each detected tumble we investigate whether a tumble was detected in previous Nc (where we set Nc =3 here) consecutive frames. If we observe multiple tumbles within Nc consecutive frames, we only consider the tumble with the maximum angular displacement.

Robotic swarm algorithms:

To test whether the idea of reduced tumbling in complex environments can help swarm based searches we used the NetLogo [33] simulation environment. In it, each robot is equipped with two sensors, one for sound / smell (to identify victims (attractants)) and the other locally senses neighboring agents or obstacles in the environment (visually, usually within a small fixed range). The simula-tion setup is shown in Figure 5a. To test the performance of different tumbling based methods in this environment we used DPSO [34]. In DPSO, to simulate natural selec-tion, many simultaneous, parallel PSO algorithms are performed on a test problem. Similar to chemotaxis models, the agents continuously adjust their movement direction based on the sound / smell gradient from the victim and their perception of the obstacles. Each robot can also influence the movement direction of other members of the swarm by sending messages about its current state. Robots then combine these messages with their own perception of the environment to determine the direction of their movement.

1. Wadhams, G. H., and Armitage J. P., (2004). Making sense of it all: bacterial chemotaxis, Nat. Rev. Mol. Cell Biol.,12: p1024.
2. Colin R,and Sourjik V. (2017). Emergent properties of bacterial chemotaxis pathway. Curr Opin Microbiol.; 39:24-33.
3. Wong-Ng J, Celani A, and Vergassola M. (2018). Exploring the function of bacterial chemotaxis. Curr Opin Microbiol.;45:16-21.
4. Harshey R. M., Kawagishi I., Maddock J., and Kenney L. J. (2003). Function, Diversity, and Evolution of Signal Transduction in Prokaryotes, Developmental Cell, 4.4:459465.
5. Waters, C. M., Bassler, B. L. (2005). Quorum sensing: cell-to-cell communication in bacteria. Annu. Rev. Cell Dev. Biol., 21, 319-346.
6. Long, Z., Quaife B., Salman, H. and Oltvai, Z.N. (2017) Cell-cell communication enhances bacterial chemotaxis toward external attractants. Sci. Rep., 7:12855
7. Tindall, M. J., Porter, S. L., Maini, P. K., Gaglia, G. and Armitage, J. P. (2008). Overview of mathematical approaches used to model bacterial chemotaxis I: the single cell, Bull. Math. Biol., 70.6:15251569.
8. Muller, S. D., Marchetto, J., Airaghi, S., and Kournoutsakos, P. (2002). Optimization based on bacterial chemotaxis. IEEE transactions on Evolutionary Computation 6.1: 16-29.
9. Chen, H., Zhu, Y., and Hu, K (2009). Cooperative bacterial foraging optimization. Discrete Dynamics in Nature and Society, 2009.
10. Lapidus, I. R., and Schiller, R (1974). A mathematical model for bacterial chemotaxis. Biophysical journal, 14.11 : 825-834.
11. Keller, E. F., and Segel, L. A. (1971). Model for chemotaxis. Journal of theoretical biology, 30.2: 225-234.
12. Shklarsh, A., Ariel, G., Schneidman, E., Ben-Jacob, E. (2011). Smart swarms of bacteria-inspired agents with performance adaptable interactions. PLoS comp. bio., 7(9), e1002177.
13. Singh, S., Rashid, S., Navlakha, S., and Bar-Joseph, Z. (2016). Distributed Gradient Descent in Bacterial Food Search, 20th Annu Conf on Res in Comp and Mol Biol (RECOMB).
14. Berg, H. C., and Brown, D. A. (1972). Chemotaxis in Escherichia coli analysed by three-dimensional tracking. Nature, 239.5374: 500-504.
15. Naghsh, A. M., Gancet, J., Tanoto, A., and Roast, C. (2008). Analysis and design of human-robot swarm interaction in firefighting. Robot and human interactive communication (RO-MAN), the 17th IEEE Intl Symp on. IEEE.
16. Vásárhelyi, G., Virágh, C., Somorjai, G., Nepusz, T., Eiben, A. E., & Vicsek, T. (2018). Optimized flocking of autonomous drones in confined environments. Science Robotics, 3:eaat3536.
17. Bearon, R. N., and Pedley, T. J. (2000). Modelling run-and-tumble chemotaxis in a shear flow. Bulletin of mathematical biology, 62.4:775.
18. Navlakha, S. and Bar-Joseph, Z. (2011). Algorithms in nature: the convergence of systems biology and computational thinking, Mol. Syst. Biol., 7:546.

19. Tero, A., Takagi, S., Saigusa, T., Ito, K., Bebber, D.P., Fricker, M.D., Yumiki, K., Kobayashi, R. and Nakagaki, T., (2010). Rules for Biologically Inspired Adaptive Network Design, Science, 327.5964:439442.
20. Galajda, P., Keymer, J., Chaikin, P., Austin, R. (2007) A wall of funnels concentrates swimming bacteria. J Bacteriol 189.23:8704–8707.
21. Wu, X.L. and Libchaber, A., (2000). Particle diffusion in a quasi-two-dimensional bacterial bath. Physical review letters, 84.13:3017.
22. Vela-Pérez, M., Fontelos, M. A., and Garnier, S. (2015). From individual to collective dynamics in Argentine ants (Linepithema humile). Mathematical biosciences, 262:56-64.
23. Anke, O., Balazsi, G., and Moss, F. (2003). Pattern formation and stochastic motion of the zooplankton Daphnia in a light field. Physica A: Stat Mech and its Appl 325.1-2: 260-66.
24. Zaburdaev, V. Y. (2006). Random walk model with waiting times depending on the preceding jump length. Journal of Statistical Physics, 123.4: 871-881.
25. Keymer, J. E., Galajda, P., Muldoon, C., Park, S., and Austin, R. H. (2006). Bacterial metapopulations in nanofabricated landscapes. Proc Natl Acad Sci., 103.46:17290-95.
26. Korobkova, E., Emonet, T., Vilar, J. M., Shimizu, T. S., & Cluzel, P. (2004). From molecular noise to behavioural variability in a single bacterium. Nature, 428.6982:574.
27. Berg H. C. (2004) E. coli in motion (Springer).
28. Lele, P. P., Hosu, B.G., and Berg, H.C. (2013) Dynamics of mechanosensing in the bacterial flagellar motor. Proc Natl Acad Sci U S A 110.29:11839–44.
29. Demir, M., Salman, H. (2017). Resonance in the response of the bacterial flagellar motor to thermal oscillations. Phys Rev E, 95.2:022419.
30. Carpenter, A.E., Jones, T.R., Lamprecht, M.R., Clarke, C., Kang, I.H., Friman, O., Guertin, D.A., Chang, J.H., Lindquist, R.A., Moffat, J. and Golland, P. (2006) CellProfiler: image analysis software for identifying and quantifying cell phenotypes. Genome Biol, 7.10:R100.
31. Jaqaman, K., Loerke, D., Mettlen, M., Kuwata, H., Grinstein, S., Schmid, S.L. and Danuser, G. (2008). Robust single-particle tracking in live-cell time-lapse sequences, Nat Methods;5.8:695-702.
32. Hastie, T., Tibshirani, R., Friedman, J., Hastie, T., Friedman, J., Tibshirani, R. (2009). The elements of statistical learning, 2(1). New York: springer.
33. Wilensky, U. (2008). NetLogo 4.0. 4.
34. Couceiro, M.S., Martins, F.M., Rocha, R.P. and Ferreira, N.M. (2014). Mechanism and convergence analysis of a multi-robot swarm approach based on natural selection. Journal of Intelligent & Robotic Systems, 76.2 : 353-381.
35. Couceiro, M.S., Vargas, P.A., Rocha, R.P. and Ferreira, N.M.(2014). Benchmark of swarm robotics distributed techniques in a search task. Robotics & Autonomous Syst. 62.2:200-13.
36. Block, S.M., Segall, J.E. and Berg, H.C., (1983). Adaptation kinetics in bacterial chemotaxis. Journal of bacteriology, 154(1):312-323.